OpenNano 7 (2022) 100045

Contents lists available at ScienceDirect

OpenNano

journal homepage: www.elsevier.com/locate/onano

QBD approach for the development of hesperetin loaded colloidal nanosponges for sustained delivery: *In-vitro, ex-vivo*, and *in-vivo* assessment

Kitty Rodrigues [a,1], Sameer Nadaf [b,1], Nilesh Rarokar [d,1], Nilambari Gurav [c], Pradnya Jagtap [e], Prashant Mali [f], Muniappan Ayyanar [g], Mohan Kalaskar [h], Shailendra Gurav [a,*]

[a] *Department of Pharmacognosy, Goa College of Pharmacy, Goa University, Panaji, Goa 403 001, India*
[b] *Sant Gajanan Maharaj College of Pharmacy, Chinchewadi, Mahagaon, Maharashtra 416503, India*
[c] *PES's Rajaram and Tarabai Bandekar College of Pharmacy, Goa University, Ponda, Goa 403 401, India*
[d] *Department of Pharmaceutical Sciences, RTM University, Nagpur, Maharashtra 440 033, India*
[e] *PDEA's S. G. R. S. College of Pharmacy, Saswad, Pune, Maharashtra, 412 301, India*
[f] *Department of Pharmacology, Sinhagad College of Pharmacy, Pune, Maharashtra, 411 041, India*
[g] *Department of Botany, A. V. V, M. Sri Pushpam College (Affiliated to Bharathidasan University), Poondi, Thanjavur, Tamil Nadu 613 503, India*
[h] *R. C. Patel Institute of Pharmaceutical Education and Research, Shirpur, 425 405 India*

ARTICLE INFO

Keywords:
Bioavailability
Bioflavonoid
Colloidal carriers
Hesperetin
Nanosponges

ABSTRACT

Hesperetin (HT) is a polyphenolic compound with anti-carcinogenic, tumor necrosis, and anti-oxidant properties. The present study reports the fabrication, optimization, and evaluation of HT-loaded nanosponges (HTN)- based gel (HTNG) for sustained anti-inflammatory effect. HTN formulation was prepared by quasi emulsion solvent diffusion method using a 4^2 factorial design. HTN was subjected to different solid and liquid state characterizations and subsequently loaded in carbopol gel. The effects of pro-inflammatory cytokines (IL- 1β and IL-6) were evaluated using RAW 264.7 macrophage cells, and the anti-inflammatory potential was tested in rats. Tiny, porous, and spherical HTN retarded the drug release (39.98%) up to 8 h compared to the pure drug (70.74%) and physical mixture (73.72%) and followed the Higuchi-matrix model. HTNG had a strong downregulating effect on cytokines. It showed no skin irritation and 18.52% skin permeation at 8 h. Further, HTNG-treated rats exhibited 33.16% inflammation inhibition compared to the control group. In conclusion, nanosponges significantly retarded the topical delivery and could circumvent the bioavailability issues associated with HT.

Abbreviations: QBD, Quality by design; HT, Hesperetin; HTN, Hesperetin-loaded nanosponges; HTNG, Hesperetin nanosponges loaded gel; HTG, Hesperetin-loaded gel; PVA, Polyvinyl alcohol; DCM, Dichloromethane; SEM, Scanning electron microscopy; TEM, Transmission electron microscopy; FTIR, Fourier transform infrared; IL, Interleukin; DMEM, Dulbecco's Modified Eagle's Medium; PM, Physical Mixture; LPS, Lipopolysaccharide; ELISA, Enzyme-linked immunosorbent assay; DCS, Diclofenac sodium; DMSO, Dimethyl sulfoxide; RH, Relative Humidity; EE, Entrapment efficiency; BET, Brunauer-Emmett-Teller; CDR, Cumulative drug release; PDI, Polydispersity index; P-XRD, Powder X-ray diffraction; ANOVA, Analysis of variance; FBS, Foetal Bovine Serum.

* Corresponding author.
E-mail address: shailendra.gurav@nic.in (S. Gurav).

[1] These authors contributed equally to this work.

https://doi.org/10.1016/j.onano.2022.100045
Received 9 March 2022; Received in revised form 19 April 2022; Accepted 20 April 2022
Available online 27 April 2022

1. Introduction

The most significant challenge is to regulate drug delivery using various contemporary techniques met by extensive research in the current years. Targeted drug delivery to the right place in test animals and controlling the flawless release of nano drugs are two major complications in nano-drug delivery [1]. Nanosponges are tiny inert colloidal structures with cavities and mesh-like structures designed for proficient and target site-specific delivery of pharmaceutical bioactives [2]. It also enables the modified drug to be released at the minimum dose and enhances stability [3].

Hesperetin (3′,5,7-trihydroxy-4-methoxyflavanone) (HT), a flavanone class of flavonoid, derived from the hydrolysis of hesperidin (hesperetin 7-rhammnoglucoside) found in citrus fruits [4]. HT is metabolized by cytochrome P450, suggesting its O-demethylation in the liver. The first-pass metabolism of HT in intestinal cells forms hesperetin 7-O-glucuronide and 3′-O-glucuronide as major HT metabolites detected in urine but not in faeces samples, signifying further bacterial growth degradation to ring fission products and phenolic acids in the colon [5]. A shorter half-life and quick clearance of HT from the body compels its frequent administration to sustain the steady plasma concentration and confer its clinical efficacy [6]. HT has vitamin-like activity and can decrease capillary permeability (vitamin P), leakiness, and fragility. Furthermore, it also exerts various biological activities such as anti-oxidant, anti--inflammatory, anti-platelet, hepatoprotective, anti-viral, anti-cancer, and neuroprotective properties [6,7]. However, despite the tremendous medicinal potential, lipophilic nature, low water solubility, and shorter half-life of HT limit its use for therapeutic interventions [8].

Notably, previous works demonstrated that the colloidal nanocarriers could improve solubility, modify release, and are responsible for enhanced bioavailability [9]. In addition, it helps to increase the drug's half-life in the systemic circulation. Due to the high surface-to-volume ratio, it also aids in tunning the basic biopharmaceutical properties of the drug; nanosponges are one of them [10]. Topical drug delivery through nanosponges offers unique advantages such as nanometric size with a 3-dimensional network, porosity, programmable release, encapsulation of hydrophilic and lipophilic drugs, targetability, and greater patient compliance, minimized dosing frequency and lesser side effects, etc. [11]. Further, the self-sterilizing nature, high entrapment efficiency, ease in scale-up, compatibility with other components, high stability over a pH range of 1–11, and temperatures up to 300 °C make them more favorable than other carriers [10,11]. Hence, nanosponges as a colloidal structure could potentially solve the biopharmaceutical problems associated with drug-like HT.

Hitherto, no study about the formulation of colloidal carrier-based sustained-release medication for HT delivery has been reported. Hence, the present investigation aims to design ethyl cellulose porous nanosponges as a colloidal carrier for the topical delivery of HT. Furthermore, it was hypothesized that the designed novel carrier is suitable for preventing the unwarranted accrual of the drug in the skin, improving its therapeutic efficacy and systemic absorption, and reducing side effects and dosing frequency.

2. Materials and methods

2.1. Materials

Hesperetin drug was purchased from Otto, Chemika, Biochemika Reagents, Mumbai, India. Ethylcellulose was procured from High Purity Laboratory Chemicals, Mumbai. Polyvinyl alcohol (PVA), Carbopol 934P, and dichloromethane (DCM) were procured from SD Fine-Chemicals Limited, Mumbai, India. All other chemicals and solvents used were of analytical grade. Double distilled water was used throughout the experimentation.

2.2. Preparation of HT nanosponges (HTN)

The HTN was prepared using a quasi emulsion solvent diffusion method using a factorial design approach. Drug: polymer ratios (X_1) (1:1, 1:4 or 1:7), solvent volume (X_2) (2, 5 or 8 mL), PVA concentrations (X_3) (30, 40 or 50 mg), stirring time (X_4) (60, 90 or 120 min) were used as independent variables, whereas % yield (Y_1), drug content (Y_2) and entrapment efficiency (Y_3) as a response. Briefly, the internal phase was prepared by dissolving ethylcellulose and HT at a predetermined ratio (1:1–1:7) into DCM (2–8 mL). Next, the internal phase was added gradually to the external phase comprised of water (20 mL) and PVA (30–50 mg) with continuous stirring at 500 rpm for 1–2 h. DCM was then removed by evaporation, the mixture was filtered, and separated nanosponges were dried in a hot air oven (Remi, Mumbai, India) at 40 °C for 24 h [11].

2.3. Drug content and entrapment efficiency determination

HTN powder equivalent to 10 mg of HT was dissolved in 50 mL ethanol and suitably diluted to obtain a 20 μg/mL concentration, then determined sample absorbance using a UV-visible spectrophotometer (Shimadzu, UV-2700). Further, the drug content and entrapment efficiency were calculated using the following equations [11];

$$\text{Drug content } (\%) = \text{Mact} / \text{Mms} \times 10 \quad (1)$$

$$\text{Entrapment efficiency } (\%) = \text{Mact} / \text{Mthe} \times 100 \quad (2)$$

where; M_{act} is the actual amount of HT in HTN, M_{ms} is the weighed quantity of HTN powder, and M_{the} is the theoretical amount of HT in

the HTN.

2.4. Photomicroscopy

A drop of the aqueous suspension was mounted on a slide and covered with a coverslip. Microscopic views of the HTN powder were recorded using an optical microscope equipped with a camera (Nikon - Eclipse E200) at a magnification of 40X [12].

2.5. Scanning electron microscopy (SEM) and transmission electron microscope (TEM)

The surface topography of the HTN was studied using a scanning electron microscope (Zeiss EVO special edition) and a transmission electron microscope (JEOL JEM-2100) [13,14]. Detailed procedures of SEM and TEM are given in the supplementary file.

2.6. Fourier transform infrared (FT-IR) studies

FT-IR spectra of HT, ethylcellulose, physical mixture (PM) of HT and ethylcellulose, and HTN were recorded using FT-IR (IR Affinity-1, Shimadzu) spectrophotometer [14] (Supplementary file).

2.7. X-ray diffraction studies

An X-ray diffraction study was performed to determine the crystalline properties of HT, PM, and HTN using X-ray diffractometer (Rigaku Ultima IV) [14] (Supplementary File).

2.8. Particle size and zeta potential analysis

HTN formulation was subjected to particle size distribution using photon correlation spectroscopy and zeta potential analysis using Smoluchowski's equation as per the reported methods [15] (Supplementary File).

2.9. Porosity analysis

The porous properties of HTN were determined using Mercury Intrusion Porosimeter (Quantochrome Nova Station A) using adsorption-desorption isotherms. The specific surface area was determined using multipoint Brunauer Emmekte Teller (BET) method. Adsorption/desorption isotherm was used to determine the pore size analysis, and by considering the pores, the pore volume and pore radius were calculated [16].

2.10. Dissolution studies

The *in-vitro* dissolution study of HTN was performed ($n = 3$) in USP type-II dissolution test apparatus (Electrolab, Mumbai, India) at 37 ± 0.5 °C; 100 rpm using phosphate buffer pH 7.4 (900 mL) as a dissolution medium. Samples were withdrawn at predetermined intervals, and sink conditions were maintained by replenishing with an equal volume of fresh medium. The samples were filtered through a 0.45 μ membrane filter and analyzed using a UV spectrophotometer at 203 nm [9,12]. The amount of HT released (%) was estimated using calibration curve equation $y = 0.037x + 0.008$ ($R^2 = 0.998$). Data analysis was accomplished using PCP Disso Software, Version -3 (Poona College of Pharmacy, India).

2.11. Preparation of HT nanosponge loaded gel (HTNG)

A total of four batches (B1-B4) of HTNG were prepared by varying the concentration of carbopol from 1 to 2.5% (Table 1). Briefly, Carbopol 934P was initially soaked in water separately for 2 h and homogenously dispersed by agitation at 600 rpm using a magnetic stirrer. Then, triethanolamine (2% v/v) was added to neutralize the pH. Finally, propylene glycol and N-methyl-2-pyrrolidone were added to this aqueous dispersion as permeation enhancers. Methylparaben (0.1%) and propylparaben (0.01%) were dissolved in distilled water (10 mL) and transferred to previously soaked carbopol 934P. Further, the mixture was agitated at 500 rpm using a

Table 1
Batches of gel formulation.

INGREDIENTS	B1	B2	B3	B4
Carbopol 934	1.0%	1.5%	2.0%	2.5%
Drug concentration	1%	1%	1%	1%
Propylene glycol	2.5%	2.5%	2.5%	2.5%
Triethanolamine	q.s	q.s	q.s	q.s
Methyl paraben	0.1%	0.1%	0.1%	0.1%
Propyl paraben	0.01%	0.01%	0.01%	0.01%
Distilled water	q.s	q.s	q.s	q.s

magnetic stirrer until smooth dispersion formed. The resultant viscous solution was kept undisturbed for 15 min and then neutralized using triethanolamine (2% v/v). To this, ethanolic solution of HT (1%) and HTN (1% w/w equivalent to HT) were added separately to form HT-loaded gel (HTG) and HTNG, respectively. Prepared gels were filled in aluminium tubes and stored at room temperature [12, 17]. The detailed composition of prepared gels is shown in Table 1.

2.12. Evaluation of gel

Prepared gels, i.e., HTG and HTNG, were evaluated visually for consistency, color, and homogeneity.

2.12.1. pH determination

The pH of the prepared HTNG was measured in triplicate using a pH meter. The electrode tip was deeped in a gel, and the results were recorded after two min [17,18].

2.12.2. Spreadability

To determine the spreadability, weighed quantity of sample was sandwiched between glass slides, and a load of 0.5 kg was placed on it. After five min, the diameter of spread circles with or without load was measured and compared [12,17].

2.12.3. In-vitro release studies

The *in-vitro* release study of HTG and HTNG was performed using Franz-diffusion cells. The dialysis membrane was soaked overnight in phosphate buffer with pH 6.8. About 1 g of gel was spread on the dialysis membrane. The receptor compartment was filled with phosphate buffer pH 6.8 (50 mL), stirred on a magnetic stirrer at 150 rpm to ensure homogeneity, and maintained at 37 ± 0.5 °C. Five ml of sample was withdrawn at predetermined intervals and analyzed spectrophotometrically at 203 nm [12,17]. Sink conditions were maintained by compensating for the equal volume of fresh buffer.

2.13. Biological studies

2.13.1. Cytokine assay

RAW 264.7 macrophage cells were cultured with Dulbecco's Modified Eagle's Medium (DMEM) containing high glucose, 2 mM Glutamine, and 10% Foetal Bovine Serum (FBS). Cells were seeded at a 1×10^5/mL density in culture plates. Further, cells were treated with lipoplysacchardie (LPS) (1 μL) and the concentrations (25–100 μg/mL) of HT, HTN, and diclofenac sodium (DCS) as standard. Cells treated with LPS and 0.1% dimethyl sulfoxie (DMSO) (LPS-only treated cells) were considered a positive control, and those treated only with 0.1% DMSO were considered a negative control. After 24 h, the supernatants were collected. The level of secretion of IL-1β and IL-6 was estimated using enzyme-linked immunosorbent assay (ELISA) kits as specified in the manufacturer's protocols [19].

2.14. In-vivo studies

2.14.1. Animals

Healthy Wistar rats of either sex weighing between 150–200 g were procured from the central animal house and kept under standard conditions (20–25 °C/55–65%RH). The animals were allowed to access rat feed and water *ad-libitum* during the acclimatization period of seven days before the commencement of the experiment. *In-vivo* experiments were conducted per the Institutional Animal Ethical Committee's standard guidelines.

2.14.2. Primary skin irritation studies

A skin irritation test was performed on Wistar albino rats ($n = 6$). The back hairs of each rat were removed using a trimmer, and an area of 4 cm^2 was marked. The rats were arbitrarily alienated into two groups ($n = 6$); Group- I: Control (gel without drug) and Group-II: treated with HTNG. The control and gel formulations were applied for seven consecutive days. The rat skin was cleaned before applying each dose and monitored after 1, 3, 5, and 7 days for reactions such as erythema and edema [20,21].

2.14.3. Ex-vivo permeation study

Ex-vivo permeation studies of HTG and HTNG were performed on the excised skin of Wistar albino rats ($n = 3$) using Franz diffusion cells as per the reported method [12,19,22]. The detailed procedure of *ex-vivo* permeation studies is given in the supplementary file.

2.14.4. In-vivo anti-inflammatory studies

The anti-inflammatory efficacy of HTNG was evaluated compared to HT and blank gel (control) using the carrageenan-induced rat paw edema method [23]. Animals were divided into four groups, each comprising five rats. 0.1 mL of 1% w/v carrageenan (1% w/v) was injected into the sub-planter region of the hind paw to induce the inflammation. The paw baseline volume was recorded by water displacement technique using a plethysmometer at 0 h before carrageenan injection and then subsequently at discrete intervals of 1, 2, 4, 6, and 8 h. The topical formulations, 0.2 g of each treatment, were applied to the surface of the right hind paw. The control group (Group 1) received a blank gel formulation, whereas Group 2, 3, and 4 were subjected to HTG, HTNG, and standard Diclofenac 5% gel. The results are expressed in terms of the mean increase in the paw volume and anti-inflammatory efficacy in terms of the percent inhibition of the edema compared with control. The two-way analysis of variance (ANOVA) test performed the statistical analysis

followed by the Bonferroni post-test [24,25].

3. Results and discussion

3.1. Formulation and optimization of HTN

A structured experimental design matrix with nineteen experiments was built according to 4^2 factorial design to determine the impact of four independent variables at their predetermined levels on the percentage yield, drug content, and entrapment efficacy (Table 2). The effects of various independent variables on the responses Y_1, Y_2, and Y_3 are illustrated using Pareto charts (Fig. S1) and 3D surface response plots (Fig. 1). A very close agreement between the experimental and predicted values indicates the design's success in evaluating and optimizing the formulations.

3.2. Effect of variables on yield (%)

The % yield for all the nineteen batches was in the broad range of 60.45 to 94.75%. The study results show that the drug: polymer ratios have a negative effect on the response Y_1. The Pareto chart and 3D response plot shown in Fig. 1 and Fig. 2, respectively show that the response Y_1 is negatively influenced by the drug: polymer ratios. It means the increased drug-polymer ratio results in an increase in % yield. The following Eq. (1) also represents the negative influence of the drug: polymer ratios on the % yield. Eq. (1) also stated the positive influence of solvent volume, emulsifier (PVA) concentrations, and stirring time on the response Y_1.

$$Y_1 = +77.79 - 6.74X_1 + 3.99X_2 + 0.0375X_3 + 0.3250X_1X_2 - 3.09X_1X_3 - 0.6187X_2X_3 + 4.14X_1X_2X_3 \quad (1a)$$

where, Y_1 is % yield and X_1, X_2, X_3, and X_4 are the drug: polymer ratios, solvent volume, emulsifier (PVA) concentrations, and stirring time, respectively.

It can be inferred that two linear [X_1 and X_2] and two interaction [X_1X_3 and $X_1X_2X_3$] terms exhibited a significant ($p < 0.05$) effect on % yield. Therefore, factors demonstrating $p > 0.05$ were considered non-significant and excluded.

Based on the results, it can be confirmed that drug: polymer ratio and DCM volume exhibited significant effects on % yield at $p < 0.05$. Drug: polymer ratio showed a more noticeable impact on Y_1 than the DCM, revealed by its relatively larger F value (38.50) (Table 3).

3.3. Effect of variables on drug content (%)

The drug content (Y_2) for nineteen different batches with different combinations of a drug to polymer ratio shows between the range of 23.51 to 74.23. Figs. 1 and 2 illustrate the Pareto chart and 3D response plot, respectively. Both the plots are evident of the positive influence of the drug: polymer ratios, emulsifier (PVA) concentrations, and stirring time on the drug content, whereas solvent volume shows a negative effect on the drug content, which means the increase in solvent volume results into the decrease in drug content and vice versa.

$$Y_2 = +46.73 + 14.12X_1 - 2.40X_2 + 1.21X_3 - 3.13X_4 - 1.72X_1X_2 - 1.22X_1X_3 - 2.91X_1X_4 + 4.29X_2X_3 + 0.7544X_2X_4 + 4.58X_3X_4 + 2.38X_1X_2X_3 - 1.67X_1X_2X_4 + 2.27X_1X_3X_4 + 5.18X_2X_3X_4 + 6.67X_1X_2X_3X_4 \quad (2a)$$

Table 2
Formulation batches of HTN.

HTN Formulation Code	Drug: Polymer Ratio	Solvent Volume (mL)	PVA Conc. (mg)	Stirring Time (min)	% yield	Drug Content (%)	EE (%)
F1	1	8	50	120	79.95	38.4	76.5
F2	7	2	30	60	79.5	70.88	80.5
F3	7	8	50	120	75.3	74.23	84.5
F4	1	2	30	60	72.8	38.29	76.5
F5	4	5	40	90	73.65	51.55	64
F6	7	2	50	60	61.4	67.52	76.5
F7	1	2	50	120	87.5	34.06	68
F8	1	2	50	60	91.55	31.76	63.5
F9	4	5	40	90	73.65	51.55	64
F10	1	8	30	120	87.7	28.06	56.1
F11	7	8	50	60	77.9	50.74	57.5
F12	1	2	30	120	74.7	25.42	50.8
F13	4	5	40	90	73.65	51.55	64
F14	1	8	30	60	93.5	25.29	50.5
F15	1	8	50	60	94.75	32.35	64.5
F16	7	2	50	120	60.45	47.27	53.5
F17	7	2	30	120	68.65	70.64	80
F18	7	8	30	60	72.75	74.81	85
F19	7	8	30	120	78.6	23.51	47

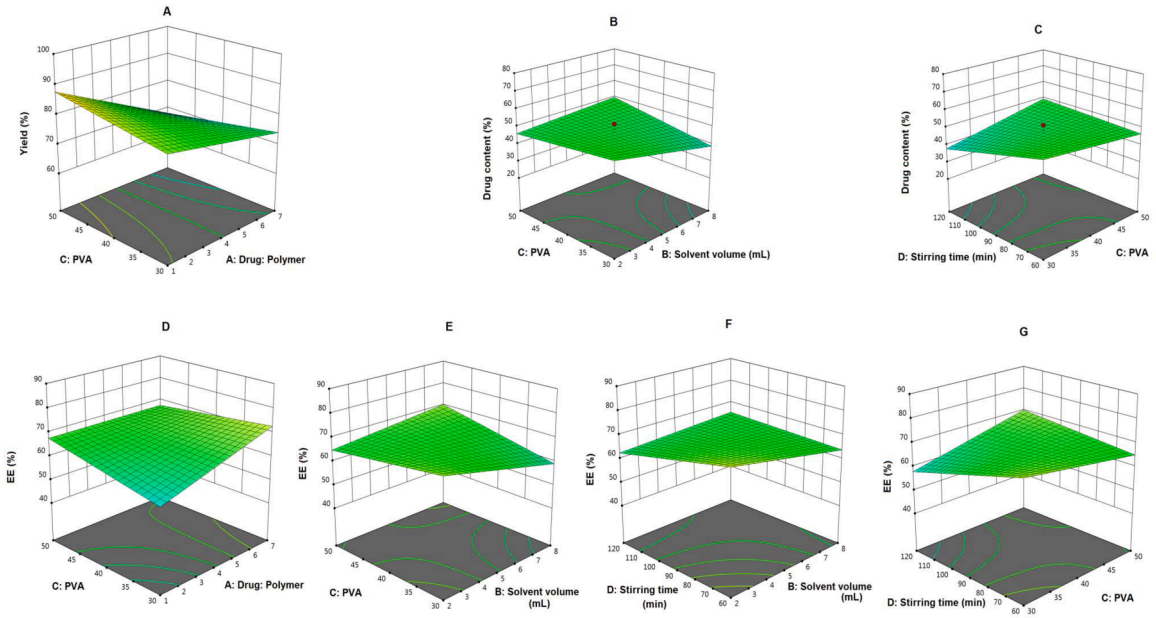

Fig. 1. 3D response plots showing effects of variables on % yield (A), drug content (B and C), and EE (D–G).

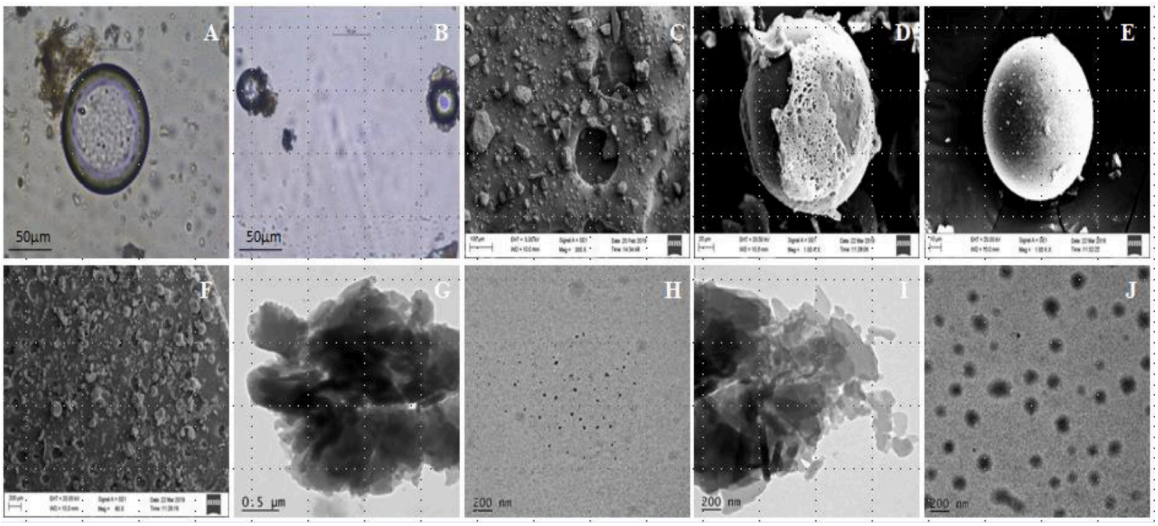

Fig. 2. Microscopic images of HTN (A and B), SEM image of HT (C) SEM image of HTN (D–F), and TEM images of HTN (G-J).

Here, one linear [X_1], two-two factor interactions [X_2X_3 and X_3X_4], one three-factor [$X_2X_3X_4$], and four-factor interaction [$X_1X_2X_3X_4$] were exhibited significant ($p < 0.05$) effects on drug content. The *F*-value of 13.70 confirms the model's statistical significance ($p < 0.05$). The value of the determination coefficient ($R^2 = 0.9856$) ensures that independent variables precisely explained 98.56% of the variation in response Y_1. Adequate precisions for the model were observed to be >4 (10.64), indicating an adequate signal, and this model can navigate the design space. ANOVA results confirmed that drug: polymer ratio exhibited a more prominent main effect on Y_2 than other factors, assigned to its relatively larger *F* value (115.70) (Table 3).

3.4. Effect of variables on EE (%)

Figs. 1 and 2 and the results obtained in the study shows that the variable X_2 and X_4 have a negative influence on the EE (Y_3), whereas the variables X_1 and X_3 show a positive effect on the EE.

$$Y_3 = +66.47 + 3.63X_1 - 1.73X_2 + 1.13X_3 - 2.38X_4 - 0.3312X_1X_2 - 3.69X_1X_3 - 1.93X_1X_4 + 4.42X_2X_3 + 3.21X_2X_4 + 4.94X_3X_4 + 0.6437X_1X_2X_3 - 1.64X_1X_2X_4 + 0.3687X_1X_3X_4 + 3.98X_2X_3X_4 + 6.96X_1X_2X_3X_4 \quad (3)$$

It can be confirmed that two linear [X_1 and X_4], four two factors [X_1X_3, X_2X_3 X_2X_4, and X_3X_4], one three-factor [$X_2X_3X_4$], and four factors [$X_1X_2X_3X_4$] interactions exhibited significant ($p < 0.05$) effect on EE (%). Furthermore, the overall results of ANOVA show the statistical significance of the model as the *p*-value was found to be less than 0.05. In contrast, the model *F* value was 23.93 with a regression coefficient (R^2) of 0.9917 (Table 3).

The optimized formulation of HTN (F18) showed 72.75%, 74.81%, and 85% yield, drug content, and entrapment, respectively. The highest entrapment was observed with a low solvent quantity. It may be attributed to the fact that a low amount of solvent produces a high-viscosity dispersed phase that obstructs the diffusion, increases droplet size, and thereby encapsulates a larger drug amount [26]. The effect of non-significant variables on % yield, drug content (%), and EE (%) is shown in Fig. S1, Fig. S2, and Fig. S3, respectively.

3.5. Characterization of HTN

Fig. 2A, B represents the spherical structures of the HTN and the polymer. The surface morphology depicted the association of drug particles with the ethylcellulose forming complexes of varying sizes and confirms the excellent entrapment of the drug into the polymer.

HT particles were observed to be irregular in shape (Fig. 2C), whereas SEM of HTN (Fig. 2D–F) depicted uniform, predominantly spherical, and highly porous nanosponges. No intact crystals were seen visually. Instead, pores were induced by solvent diffusion from the nanosponge surface. Nanosponges' cross-sectional view revealed the characteristic internal structure with a spherical cavity and void annular spaces enclosed by a rigid shell constructed from drug and polymers.

TEM results (Fig. 2G–J) confirmed a spherical shape of HTN and thus revealed the internal structure of the prepared nanosponges [11,14].

FT-IR spectrum of optimized HTN showed a characteristic band at 3329.14 cm^{-1} ascribed to hydroxyl (O–H) stretching, indicating the formation of strong hydrogen bonds (Fig. 3). The peak at 2926.01 cm^{-1} was assigned to C-H stretching. A band at 1705.07 cm^{-1} corresponds to C=O bond stretching. $–CH_3$ deformation vibration was at peak 1440.83 cm^{-1}, and 1259.5 cm^{-1} was due to asymmetric C=N bond seen in the spectrum. These results suggested drug-excipients compatibility during nanosponge preparation. Further, it confirmed drug stability and entrapment in nanosponge formulation [14,15].

The reduction in the peak intensity and peak broadening in the FT-IR spectrum of nanosponge indicates the partial solubilization of HT in the porous structure. Pores might have shown a resistance effect on the formation of crystalline counterparts and possessed drug in partial crystalline form. The spectroscopic study corroborated neither appearance of any new peak nor the disappearance of existing peaks.

The thermal behavior of the HT, PM, and HTN is depicted in Fig. 4. The thermogram of HT (Fig. 4A) exhibited a sharp endothermic peak at 230.42 °C, matching HT's melting point. In addition, the DSC curve of the PM showed the characteristic peak of the drug (Fig. 4B) [27].

The thermogram of HTN (Fig. 4C) also exhibited the HT's characteristic peak, thus confirming that the HT was stable and successfully loaded in nanosponge formulation. Furthermore, the results for HTN revealed the drug and polymer's compatibility and therefore offer the appropriateness of the preparation method [14] (Table 3).

HT's P-XRD spectra showed strong reflections at around 15, 35, and 45°, indicating its crystalline nature (Fig. 4D). The PM also retained a similar peak with almost the same intensities (Fig. 4E). However, the peak intensities were somewhat diminished in the P-XRD spectrum of HTN (Fig. 4F). Results corroborate the entrapment of HT in the partial crystalline form, in line with FT-IR studies [14].

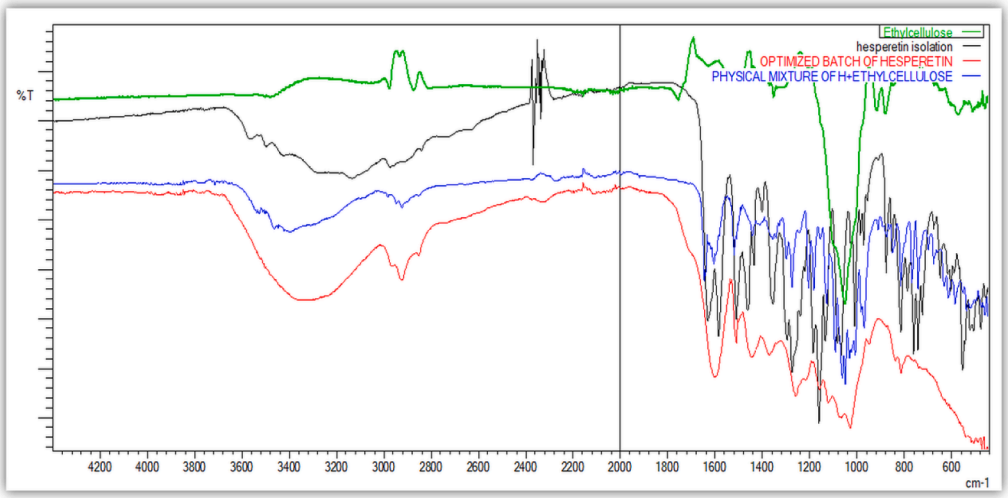

Fig. 3. FT-IR spectra of ethylcellulose (green line), HT (black line), HTN (red line), and PM (blue line).

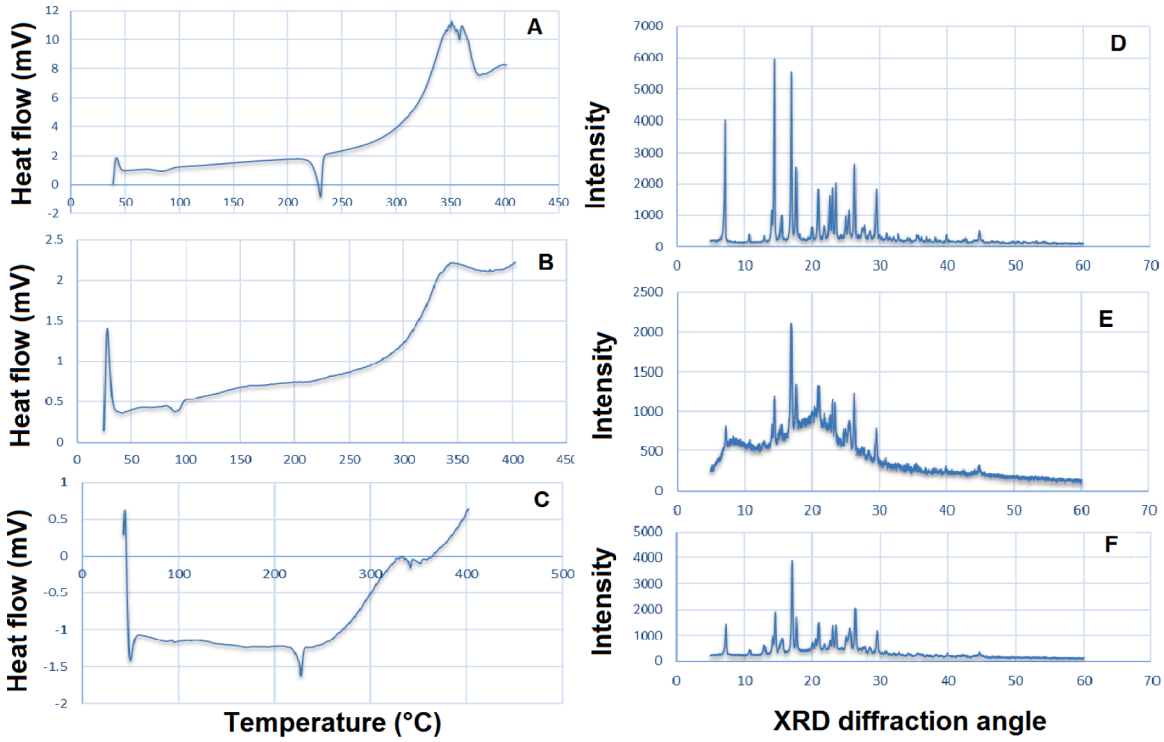

Fig. 4. Thermogram of HT (A), PM (B), and HTN (C). XRD spectrum of HT (D), PM (E), and HTN (F).

Table 3
ANOVA results for responses Y_1, Y_2, and Y_3.

Source	% yield			Drug content			EE (%)		
	Coeff.	*F*-value	*p*-value	Coeff.	*F*-value	*p*-value	Coeff.	*F*-value	*p*-value
Model/Intercept	77.79	6.12	0.0466	46.73	13.70	0.0264	66.47	23.93	0.0118
X_1-Drug: Polymer	−6.74	38.50	0.0034	14.12	115.70	0.0017	3.63	29.16	0.0124
X_2-Solvent volume	3.99	13.50	0.0213	−2.40	3.35	0.1646	−1.73	6.63	0.0822
X_3-PVA	0.0375	0.0012	0.9741	1.21	0.8554	0.4232	1.13	2.83	0.1911
X_4-Stirring time	−1.96	3.24	0.1462	−3.13	5.68	0.0974	−2.38	12.54	0.0383
X_1X_2	0.3250	0.0894	0.7798	−1.72	1.72	0.2805	−0.3312	0.2426	0.6561
X_1X_3	−3.09	8.10	0.0466	−1.22	0.8696	0.4199	−3.69	30.17	0.0119
X_1X_4	0.8875	0.6668	0.4600	−2.91	4.91	0.1135	−1.93	8.25	0.0640
X_1X_3	−0.6187	0.3241	0.5996	4.29	10.69	0.0468	4.42	43.18	0.0072
X_2X_4	−0.2125	0.0382	0.8545	0.7544	0.3301	0.6058	3.21	22.73	0.0175
X_3X_4	−0.8437	0.6027	0.4809	4.58	12.15	0.0399	4.94	54.05	0.0052
$X_1X_2X_3$	4.14	14.49	0.0190	2.38	3.29	0.1675	0.6437	0.9164	0.4090
$X_1X_3X_4$	2.09	3.71	0.1263	−1.67	1.62	0.2932	−1.64	5.97	0.0921
$X_1X_3X_4$	1.02	0.8894	0.3990	2.27	2.99	0.1822	0.3687	0.3007	0.6216
$X_2X_3X_4$	−1.34	1.51	0.2859	5.18	15.58	0.0290	3.98	35.05	0.0096
X_1 $X_2X_3X_4$				6.67	25.79	0.0147	6.96	107.00	0.0019

The particle size of HTN showed the average size as 105.08nm (Fig. S5A). The solvent volume and ethylcellulose concentration influenced the particle size of nanosponges. An increase in the ethanol volume produces a less viscous solution, resulting in smaller particle size [28]. Polydispersity index (PDI) value < 0.1 and <0.5 corresponds to the mono-disperse and poly-disperse systems, respectively. Lower PDI values show a better particle size homogeneity [29]. A polydispersity index value was 0.097, confirming mono-disperse particles with better homogeneity.

Zeta potential is known to impact the stability of colloidal dispersions. Nanosponges with zeta potentials $>+30$ mV and <-30 mV are usually considered stable and further restrain the aggregation between charged particles. The zeta potential of the prepared HTN was -1.35 mV (Fig. S5B), indicating colloidal stability [13].

BET analysis (Fig. 5A) was conducted to determine the change in porous nanosponges' specific surface area, pore-volume, and pore size distribution. The surface area *S*BET of the present porous HTN was 0.1666 nm^2/g. The pore size distribution of the nanosponge is presented in Fig. 5B, which is due to the high surface free energy and ease of filling the smaller pores. Therefore, the immersion of

nanosponges in the DCM solution leads to its absorption into the smaller pores [16].

3.6. Dissolution studies

At the end of 8 h, the dissolution studies demonstrated about 70.74, 73.72, and 39.98% of the drug releasefrom HT, PM, and HTN, respectively (Fig. 5D).

The dissolution rates of the PM and HTN were significantly different ($p < 0.05$) compared to HT. Similarly, % CDR from HTN were dissimilar ($p < 0.05$) compared to the PM. HTN retarded the HT release by 1.77 and 1.84 folds compared to HT and PM, respectively.

The release kinetics and mechanism were estimated by fitting the data into different kinetic models. Drug release from HTN ($R^2 = 0.9611$) and PM ($R^2 = 0.9247$) followed the Higuchi-matrix model. It corroborates that the HT is entrapped well within the pores, and the nanosponges can retard the HT release significantly [9,27]. A previous report on hesperetin-loaded poly(lactic-co-glycolic acid) nanoparticles observed ≈31% of the burst release at the first 2 h and 65% HT release within 24 h [30]. While HT conjugated, PEGylated gold nanoparticles released 99% of HT within 8 h [31]. These results confirmed that nanosponge could be an excellent carrier system for HT.

3.7. Characterization of HTNG

The prepared HTNG was non-opaque white with a pH of 6.42 ± 0.415 and devoid of phase separation directed the homogeneity of the preparation. Furthermore, the pH was physiologically compatible with the skin pH, consequently, it would be non-irritant, confirming the suitability of HTNG for topical application.

The determined spreadability of the HTNG was 1.7 cm which facilitated the spread within less time. The spreadability of gel decides its therapeutic efficacy. Moreover, sufficient spreading of gel ensures the uniform application of the gel to the skin. Thus, the prepared gels should exhibit excellent spreadability and fulfill the prime requirement of topical application [32].

The *in-vitro* release profile of HTNG containing different carbopol concentrations is shown in Fig. 5E. The cumulative release from HTG was determined to be 42.10% at the end of 10 h, whereas HTNG exhibited 34.91% (B1), 29.94%

(B2), 25.03 % (B3), and 40.10 % (B4) drug release. Formulation B3 was selected as an optimized formulation as it retarded the drug release to a larger extent. All the batches followed Higuchi- matrix release model ($R^2 = 0.9147–0.9458$). Significant ($p < .00001$)

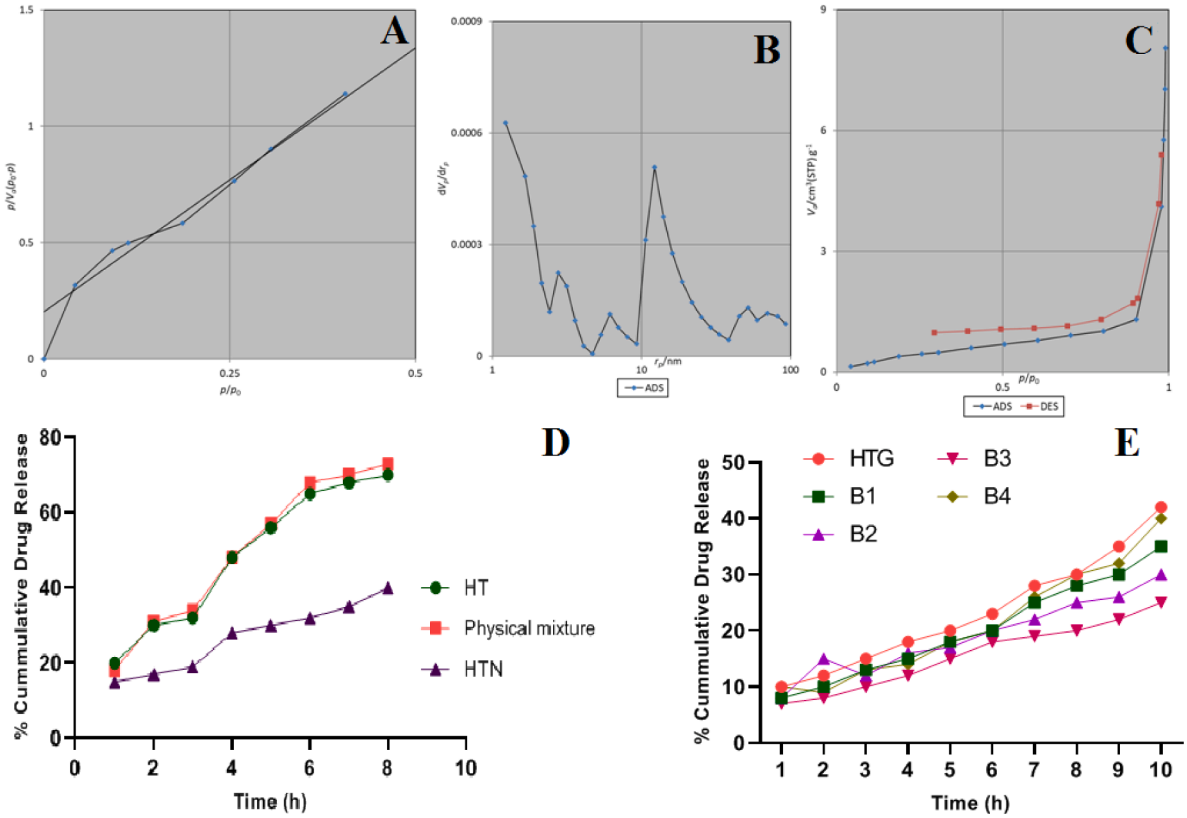

Fig. 5. BET plot (A), pore size distribution (B), and adsorption-desorption isotherm of HTN (C). Comparative dissolution study of HT, PM, and HTN (D). Graph depicting the release of HT from HTG and different batches of HTNG prepared at different concentrations (1% to 2.5%) of Carbopol 934P (E).

difference was observed between drug release retardation shown by HTG and Formulation B3 (HTNG). The concentration of Carbopol 934P exhibited a profound effect on HT release from different batches of HTNG. The drug release rates decreased as the proportion of carbopol 934P increased. It enhanced drug retention time, prohibited drug leakage, and hindered drug release for several hours. It could be due to the higher viscosity of gel achieved with high carbopol concentration and smaller gel mesh that reduced droplet movement from the gel matrix [33]. Maximum retardation of drug release was observed at a 2% concentration of Carbopol 934P. However, carbopol usage beyond 2.5% further increased the HT release. It is because carbopol forms high gel strength at low concentrations that help accomplish required drug release profiles [34].

Through secretion of different cytokines and mediators, Macrophages play a pivotal role in the instigation, continuance, and resolution of inflammatory responses [35]. Suppression of these secreted cytokines is the approach to combat inflammation. Therefore, we examined the effect of different concentrations of prepared formulation on the secretion of IL-1β and IL-6 cytokines in LPS-stimulated macrophage cells by ELISA technique and compared it with standard i.e. (DCS). As shown in Fig. 6A, LPS-treated cells exhibited high IL-1β level (68.2 ± 2.57 pg/mL) compared to the negative control (15.4 ± 0.98 pg/mL). IL-6 level increased from 65.3 ± 3.5 pg/mL (negative control) to 676.4 ± 8.57 pg/mL on treatment with LPS (Fig. 6B). Treatment of cells with different concentrations (25-100 μg/mL) of the HT and HTN downregulated IL-1β levels from 65.3 ± 1.68 pg/mL and 56.2 ± 2.52 pg/mL to 33.85 ± 1.56 pg/mL and 18.38 ± 1.2 pg/mL respectively (Fig. 6A). The same phenomenon was observed for IL-6 secretions (Fig. 6B). At each concentration, HTN exhibited a significant ($p < 0.0001$) inhibitory effect on the secretion of both IL-1β and IL-6 compared to HT. HTN and DCS showed a non-significant inhibiting effect on the secretion of IL-1β except at 75 μg/mL. However, downregulating effect demonstrated by HTN and DCS on the secretion of IL-6 was significant at $p < 0.0001$. It confirmed that HTN increased the anti-inflammatory potential of HT.

The HTNG and HTG exhibited neither erythema nor edema on the intact and abraded rat skin for seven days, confirming the non-irritancy of any formulations to the rat skin. Moreover, a smaller carbopol 934P-based gel matrix mesh prohibits droplet movement to the deep skin layers, thereby diminishing skin irritation [33].

The *ex-vivo* study was carried out for the HTG and HTNG. The results obtained during the study show that about 23.32% drug was permeated (Fig. 7A) through the rat's skin from HTG at the end of 8 h. In contrast, the HTNG powder demonstrated about 18.52% of HT permeation through rat skin in the same duration. The HTG and HTNG showed the same release rate in the initial 3 h, but after that, at the 4th hour, HTG suddenly showed a decrease in release, and again in the 5th hour, it showed a sudden increase in the release rate of HT from HTG. On the other hand, HTNG shows a sudden upsurge in release rate at the 4th hour, followed by a sustained release for several hours. HTNG exhibited a significant ($p < 0.00001$) decrease in HT permeation to HTG, and this might be owing to the dual barrier produced by the nanosponges and gelling network. Furthermore, the high proportion of carbopol might have reduced the mesh size of the gel matrix, diminished the droplet movement to nearby pores and deep layers, increased drug retention in the epidermis, and hindered the skin permeation rate [33,36]. The anti-inflammatory study of prepared formulations was assessed using the carrageenan-induced rat paw edema model.

HTNG formulation, blank gel formulation (control), HTG, and standard Diclofenac 5% gel were applied on the shaved rat skin, and their therapeutic efficacy was assessed up to 10 h. The topical application of HTNG exhibited significant ($p< 0.05$–0.01) percent inhibition of paw edema at 2, 4, 6, and 8 h after carrageenan injection ranging from 29.45, 43.90, 49.28, and 51.27% compared to the control group, whereas significant ($p< 0.05$) reduction in paw edema volume at 4 and 8 h compared to the HTNG (Fig. 7B,C). On the other hand, the standard drug Diclofenac 5% showed the maximum percentage of inhibition of paw edema, 53.86%. The results corroborated that the HTNG promoted its anti-inflammatory efficacy compared to HTG. It could be assigned to the reduced mesh size of the gel matrix, hindered droplet movement and thereby reduced skin permeation rate, gel matrix facilitated the enhancement of drug retention in epidermis, a high affinity between carbopol 934P and the *stratum cornea* [33,37].

4. Conclusion

Ethylcellulose nanosponges were prepared and screened as a carrier for topical delivery of HT. Characteristics of prepared nanosponges were influenced by different independent variables such as drug: polymer ratio, the volume of DCM, and the amount of emulsifier. Merits of prepared nanosponge-based gel such as release retardation for a more extended period, lack of significant irritation, and greater compatibility could help to reduce the dosing frequency and might cause the formulation to occupy the market in nearby future. However, further clinical studies are warranted to establish the efficacy and safety of these formulations on human skin.

Funding statement

The present research did not receive any specific grant from funding agencies in the public, commercial, or not-for-profit sectors.

CRediT authorship contribution statement

Kitty Rodrigues: Methodology, Software, Data curation, Resources. **Sameer Nadaf:** Methodology, Software, Data curation, Resources. **Nilesh Rarokar:** Writing – original draft, Visualization, Formal analysis. **Nilambari Gurav:** Conceptualization, Methodology, Writing – review & editing, Supervision, Investigation, Writing – original draft, Visualization, Formal analysis. **Pradnya Jagtap:** Software, Validation, Investigation. **Prashant Mali:** Software, Validation, Investigation. **Muniappan Ayyanar:** . **Mohan Kalaskar:** Conceptualization, Methodology, Writing – review & editing, Supervision, Investigation, Writing – original draft, Visualization, Formal analysis. **Shailendra Gurav:** Conceptualization, Methodology, Writing – review & editing, Supervision, Investigation.

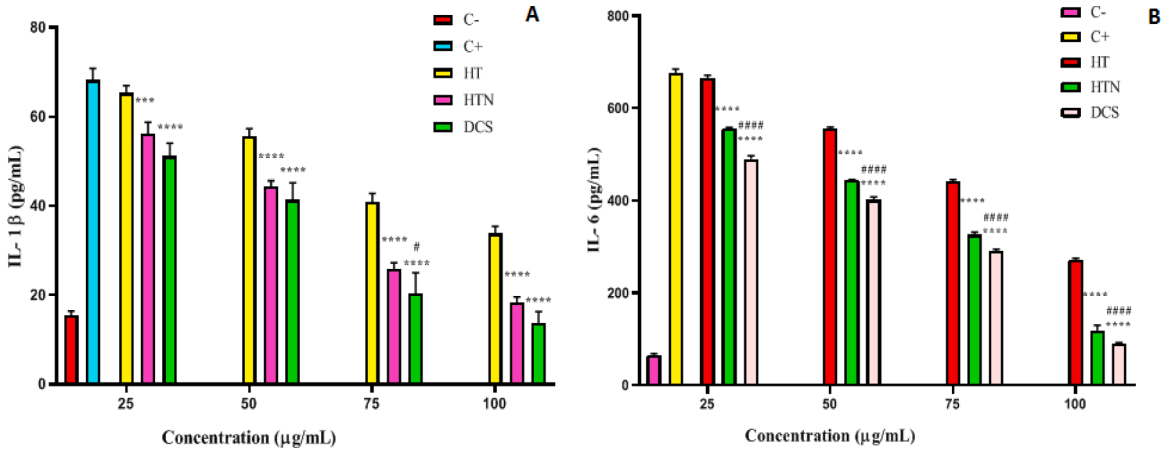

Fig. 6. Inhibitory effect of HT, HTN and DCS on the secretion of (A) IL- 1β and (B) IL-6. Data are expressed as mean ± SD values ($n = 3$). * indicates compared with HT and # indicates compared with HTN. (*p<0.05, **p<0.01, ***p <0.001, ****p<0.0001) (One way ANOVA followed by Tukey's multiple comparisons test).

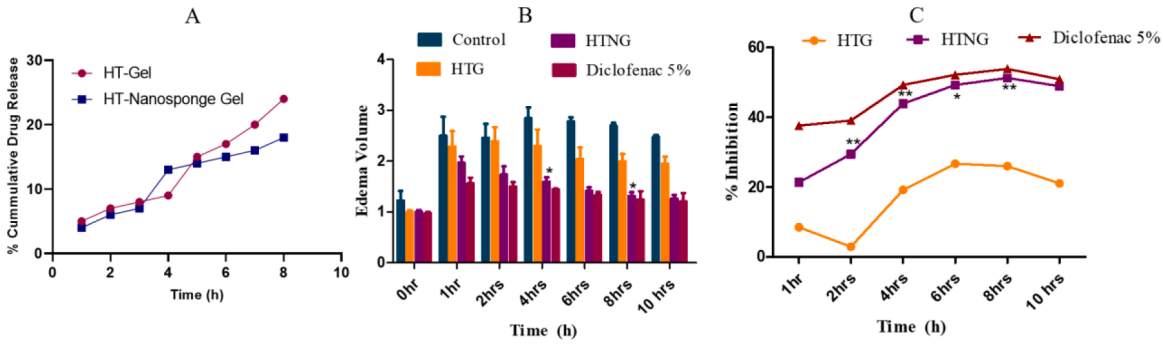

Fig. 7. (A) *Ex-vivo* permeability study of HTNG. (B) Effect of formulations on the paw edema volume. The results represent mean ± SEM ($n = 6$). *$p < 0.05$ compared to the HTG. (C) *In-vivo* anti-inflammatory studies of HTNG and HTN (*$p < 0.05$ and **$p < 0.01$ compared with HTG. Values are expressed as Mean + SEM).

Declaration of Competing Interest

The authors declare that there is no conflict of interest in this work.

Supplementary materials

Supplementary material associated with this article can be found, in the online version, at doi:10.1016/j.onano.2022.100045.

Referencess

[1] A. Jain, S.K. Jain, *In vitro* release kinetics model fitting of liposomes: an insight, Chem. Phys. Lipids 201 (2016) 28–40, https://doi.org/10.1016/j.chemphyslip.2016.10.005.
[2] P. Pandey, D. Purohit, H. Dureja, Nanosponges–a promising novel drug delivery system, Recent Pat. Nanotechnol. 12 (3) (2018) 180–191.
[3] M. Shringirishi, S.K. Prajapati, A. Mahor, S. Alok, P. Yadav, A. Verma, Nanosponges: a potential nanocarrier for novel drug delivery-a review, Asian Pac. J. Trop. Dis. 4 (2014) S519–S526, https://doi.org/10.1016/S2222-1808(14)60667-8.
[4] J. Cho, Antioxidant and neuroprotective effects of hesperidin and its aglycone hesperetin, Arch. Pharm. Res. 29 (2006) 699–706, https://doi.org/10.1007/BF02968255.
[5] A. Roohbakhsh, H. Parhiz, F. Soltani, R. Rezaee, M. Iranshahi, Neuropharmacological properties and pharmacokinetics of the citrus flavonoids hesperidin and hesperetin—a mini-review, Life Sci. 113 (1-2) (2014) 1–6, https://doi.org/10.1016/j.lfs.2014.07.029.
[6] I. Erlund, Review of the flavonoids quercetin, hesperetin, and naringenin, dietary sources, bioactivities, bioavailability, and epidemiology, Nutr. Res. 24 (10) (2004) 851–874, https://doi.org/10.1016/j.nutres.2004.07.005.
[7] X. Guo, X. Cao, X. Fang, A. Guo, E. Li, Involvement of phase II enzymes and efflux transporters in the metabolism and absorption of naringin, hesperidin and their aglycones in rats, Int. J. Food Sci. Nutr. (2021) 1–11, https://doi.org/10.1080/09637486.2021.2012562.

[8] K. Chadha, M. Karan, Y. Bhalla, R. Chadha, S. Khullar, S. Mandal, K. Vasisht, Cocrystals of hesperetin: structural, pharmacokinetic, and pharmacodynamic evaluation, Cryst. Growth Des. 17 (5) (2017) 2386–2405, https://doi.org/10.1021/acs.cgd.6b01769.
[9] N. Rarokar, C. Ravikumar, S. Gurav, P. Khedekar, Meloxicam encapsulated nanostructured colloidal self-assembly for evaluating antitumor and anti-inflammatory efficacy in 3D printed scaffolds, J. Biomed. Mat. Res. 109 (8) (2020) 1441–1456, https://doi.org/10.1002/jbm.a.37135.
[10] K. Tiwari, S. Bhattacharya, The ascension of nanosponges as a drug delivery carrier: preparation, characterization, and applications, J. Mater. Sci. Mater. Med. 33 (28) (2022), https://doi.org/10.1007/s10856-022-06652-9.
[11] S. Kumar, M. Prasad, R. Rao, Topical delivery of clobetasol propionate loaded nanosponge hydrogel for effective treatment of psoriasis: formulation, physicochemical characterization, antipsoriatic potential and biochemical estimation, Mater. Sci. Eng. C 119 (2021), 111605, https://doi.org/10.1016/j.msec.2020.111605.
[12] K. Rodrigues, S. Gurav, A. Joshi, M. Krishna, A. Bhandarkar, Porous polymeric carrier system for modified drug release of boswellic acid, Chem. Sci. J. 11 (2) (2020) 1–12, https://doi.org/10.37421/csj.2020.11.210.
[13] S. Dessai, M. Ayyanar, S. Amalraj, P. Khanal, S. Vijayakumar, N. Gurav, N. Rarokar, M. Kalaskar, S. Nadaf, S. Gurav, Bioflavonoid mediated synthesis of TiO_2 nanoparticles: characterization and their biomedical applications, Mater. Lett. (2022), 131639, https://doi.org/10.1016/j.matlet.2021.131639.
[14] S. Anandam, S. Selvamuthukumar, Fabrication of cyclodextrin nanosponges for quercetin delivery: physicochemical characterization, photostability, and antioxidant effects, J. Mater. Sci. 49 (23) (2014) 8140–8153, https://doi.org/10.1007/s10853-014-8523-6.
[15] S. Saoji, N. Rarokar, P. Dhore, S. Dube, N. Gurav, S. Gurav, N. Raut, Phospholipid based colloidal nanocarriers for enhanced solubility and therapeutic efficacy of withanolides, J. Drug Deliv. Sci. Technol. 70 (2022), 103251, https://doi.org/10.1016/j.jddst.2022.103251.
[16] B.K. Almutairy, A. Alshetaili, A.S. Alali, M.M. Ahmed, M. Anwer, M.A. Aboudzadeh, Design of olmesartan medoxomil-loaded nanosponges for hypertension and lung cancer treatments, Polymers 13 (14) (2021) 2272, https://doi.org/10.3390/polym13142272.
[17] G. Aggarwal, M. Nagpal, G. Kaur, Development and comparison of nanosponge and niosome based gel for the topical delivery of tazarotene, Pharm. Nanotechnol. 4 (3) (2016) 213–228, https://doi.org/10.2174/2211738504666160804154213.
[18] R.R. Verekar, S.S. Gurav, U. Bolmal, Thermosensitive mucoadhesive in situ gel for intranasal delivery of Almotriptan malate: formulation, characterization, and evaluation, J. Drug Deliv. Sci. Technol. 58 (2020), 101778, https://doi.org/10.1016/j.jddst.2020.101778.
[19] N. Naseri, K. Kalantar, Z. Amirghofran, Anti-inflammatory activity of *Echium amoenum* extract on macrophages mediated by inhibition of inflammatory mediators and cytokines expression, Res. Pharm. Sci. 13 (1) (2018) 73–81, https://doi.org/10.4103/1735-5362.220970.
[20] O. James, A.B. Sunday, Evaluation of acute dermal irritation and wound contraction by gymnema sylvestre and datura metel extracts in rats, Am. J. Biomed. Life Sci. 2 (4) (2014) 83–88, https://doi.org/10.11648/j.ajbls.20140204.14.
[21] S.R. Wayal, S.S. Gurav, Evaluation of wound healing potential of Bhallatakadi Ghrita-cow ghee based polyherbal formulation: *in-vivo* excision and incision wound model, J. Complement. Integr. Med. 18 (3) (2021) 507–515, https://doi.org/10.1515/jcim-2020-0179.
[22] N.A. Patel, N.J. Patel, R.P. Patel, Formulation and evaluation of curcumin gel for topical application, Pharm. Dev. Technol. 14 (1) (2009) 83–92, https://doi.org/10.1080/10837450802409438.
[23] Y. He, K. Majid, M. Maqbool, T. Hussain, A.M. Yousaf, I.U. Khan, Y. Mehmood, A. Aleem, M.S. Arshad, A. Younus, J.S. Nirwan, Formulation and characterization of lornoxicam-loaded cellulosic-microsponge gel for possible applications in arthritis, Saudi. Pharm. J. 28 (8) (2020) 994–1003, https://doi.org/10.5530/jyp.2018.2s.11.
[24] S. Gurav, V. Gulkari, N. Duragkar, S. Sakharwade, P. Itankar, A. Patil, Analgesic and anti-inflammatory activity of *Flacourtia ramontchi L.* Herit, Pharmacologyonline. 2 (2007) 20–31.
[25] S. Lalsare, P.K. Verma, M. Khatak, S. Ranjan, S. Rajurakar, S.S. Gurav, Anti-inflammatory and antimicrobial activity of Flacourtia ramontchi leaves, Int. J. Drug. Dev. Res. 3 (2) (2011) 308–313.
[26] A. Moin, T.K. Deb, R.A.M. Osmani, R.R. Bhosale, U. Hani, Fabrication, characterization, and evaluation of microsponge delivery system for facilitated fungal therapy, J. Basic Clin. Pharm. 7 (2) (2016) 39, https://doi.org/10.4103/0976-0105.177705.
[27] R. Saini, S.K. Singh, P.R.P. Verma, Evaluation of carvedilol-loaded microsponges with nanometric pores using response surface methodology, J. Exp. Nanosci. 9 (8) (2014) 831–850, https://doi.org/10.1080/17458080.2012.725258.
[28] R. Sareen, K. Nath, N. Jain, K.L. Dhar, Curcumin loaded microsponges for colon targeting in inflammatory bowel disease: fabrication, optimization, and *in vitro* and pharmacodynamic evaluation, Biomed. Res. Int. (2014) 1–7, https://doi.org/10.1155/2014/340701.
[29] E. Anwar, N. Farhana, Formulation and evaluation of phytosome-loaded maltodextrin-gum arabic microsphere system for delivery of camellia sinensis extract, J. Young Pharm. 10 (2s) (2018) S56, https://doi.org/10.5530/jyp.2018.2s.11.
[30] M. Ersoz, A. Erdemir, D. Duranoglu, D. Uzunoglu, T. Arasoglu, S. Derman, B. Mansuroglu, Comparative evaluation of hesperetin loaded nanoparticles for anticancer activity against C6 glioma cancer cells, Artif. Cells Nanomed. Biotechnol. 47 (1) (2019) 319–329, https://doi.org/10.1080/21691401.2018.1556213.
[31] G. Krishnan, J. Subramaniyan, S.P. Chengalvarayan, B. Muralidharan, D. Thiruvengadam, Hesperetin conjugated PEGylated gold nanoparticles exploring the potential role in anti-inflammation and anti-proliferation during diethylnitrosamine-induced hepatocarcinogenesis in rats, Asian J. Pharm. Sci. 12 (5) (2017) 442–455, https://doi.org/10.1016/j.ajps.2017.04.001.
[32] M. Dantas, S. Reis, C. Damasceno, L. Rolim, P. Rolim-Neto, F. Carvalho, L. Quintans-Junior, J. Almeida, Development and Evaluation of Stability of a Gel formulation containing the monoterpene borneol, Sci. World J. 2016 (2016), 7394685, https://doi.org/10.1155/2016/7394685.
[33] Y. Zheng, W. Ouyang, Y. Wei, S. Syed, C. Hao, B. Wang, Y. Shang, Effects of carbopol® 934 proportion on nanoemulsion gel for topical and transdermal drug delivery: a skin permeation study, Int. J. Nanomed. 10 (11) (2016) 5971–5987, https://doi.org/10.2147/IJN.S119286.
[34] N. Mariageraldrajan, Novel carbopol-wax blends for controlled release oral dosage forms. (2007). Theses and Dissertations (ETD). Paper 163. 10.21007/etd.cghs.2007.0201.
[35] N. Fujiwara, K. Kobayashi, Macrophages in inflammation, Curr. Drug. Targets Inflamm. Allergy. 4 (3) (2005) 281–286, https://doi.org/10.2174/1568010054022024.
[36] B. de Vargas, D. Argenta, G. Borghetti, L. Koester, V. Bassani, H. Teixeira, Validation of an LC method to determine skin retention profile of genistein from nanoemulsions incorporated in hydrogels, J. Chromatogr. Sci. 50 (2) (2012) 114–118.
[37] D. Mou, H. Chen, D. Du, C. Mao, J. Wan, H. Xu, X. Yang, Hydrogel-thickened nanoemulsion system for topical delivery of lipophilic drugs, Int. J. Pharm. 353 (1) (2008) 270–276, https://doi.org/10.1016/j.ijpharm.2007.11.051.